Heliyon 10 (2024) e23721

Contents lists available at ScienceDirect

Heliyon

journal homepage: www.cell.com/heliyon

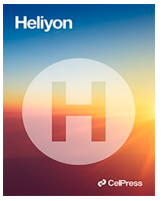

One-step hydrothermal synthesis of CuS/MoS_2 composite for use as an electrochemical non-enzymatic glucose sensor

Krishna Prasad Sharma [a], Miyeon Shin [a], Ganesh Prasad Awasthi [b], Soonhwan Cho [c,**], Changho Yu [a,b,*]

[a] Department of Energy Storage/Conversion Engineering (BK21 FOUR), Jeonbuk National University, Jeonju, Jeollabuk-do, 54896, Republic of Korea
[b] Division of Convergence Technology Engineering, Jeonbuk National University, Jeonju, Jeollabuk-do, 54896, Republic of Korea
[c] ENPLUS Co., LTD, 167 Jayumuyeok-gil, Baeksan-myeon, Gimje-si, 54352, Republic of Korea

ARTICLE INFO

Keywords:
Sensitivity
Selectivity
Hydrothermal
Copper sulfide
Molybdenum disulfide

ABSTRACT

Early diagnosis may be crucial for the prevention of chronic diabetes mellitus. For that herein, we prepared a CuS/MoS_2 composite for a non-enzymatic glucose sensor through a one-step hydrothermal method owing to the synergetic effect of CuS/MoS_2. The surface morphology of CuS/MoS_2 was studied by Field Emission Scanning Electron Microscopy (FESEM) and Cs-corrected Scanning Transmission Electron Microscopy (Cs-STEM). The crystallinity and surface composition of CuS/MoS_2 were analyzed by X-ray Diffraction (XRD) and X-ray Photoelectron Spectroscopy (XPS) respectively. The working electrode was prepared from CuS/MoS_2 electrocatalyst, and for that dispersed solution of electrocatalyst was used to fabricate the material-loaded glassy carbon electrode (GC). CuS/MoS_2 composite shows the viability of electrocatalyst to oxidize glucose in an alkaline solution with sensitivity and detection limit of 252.71 μA mM^{-1} cm^{-2} and 1.52 μM respectively. The proposed glucose sensor showed reasonable stability and potential selectivity during electrochemical analysis. Accordingly, the CuS/MoS_2 composite has potential as a viable material for glucose sensing in diluted human serum.

1. Introduction

Diabetes is a chronic health condition resulting from glucose metabolism disorder in the human body [1–4]. "According to the World Health Organization (WHO), the number of deaths from diabetes increased globally by 70 % between 2000 and 2019" [5]. Prevention, diagnosis, and treatment require the development of fast, reliable, and accurate tools to detect blood glucose levels. Currently, a variety of analytical techniques including colorimetric and electrochemical are being used for glucose sensing [6,7]. Nowadays, electrochemical-based methods are attracting researchers' attention due to their cost effectiveness, sensitivity, and stability. Based on enzyme use, electrochemical biosensors are classified into enzymatic and non-enzymatic biosensors. As reported by Wilson and Turner, enzymatic glucose sensors exhibit excellent selectivity and sensitivity, but poor stability at room temperature impairs their practical application [8,9]. So employing a catalyst like platinum [10], gold [11], silver [12], copper [13], as well as zinc

* Corresponding author. Department of Energy Storage/Conversion Engineering (BK21 FOUR), Jeonbuk National University, Jeonju, Jeollabuk-do, 54896, Republic of Korea.
** Corresponding author.
E-mail addresses: chodream@en3.co.kr (S. Cho), goody0418@jbnu.ac.kr (C. Yu).

https://doi.org/10.1016/j.heliyon.2023.e23721
Received 27 June 2023; Received in revised form 10 December 2023; Accepted 12 December 2023
Available online 15 December 2023

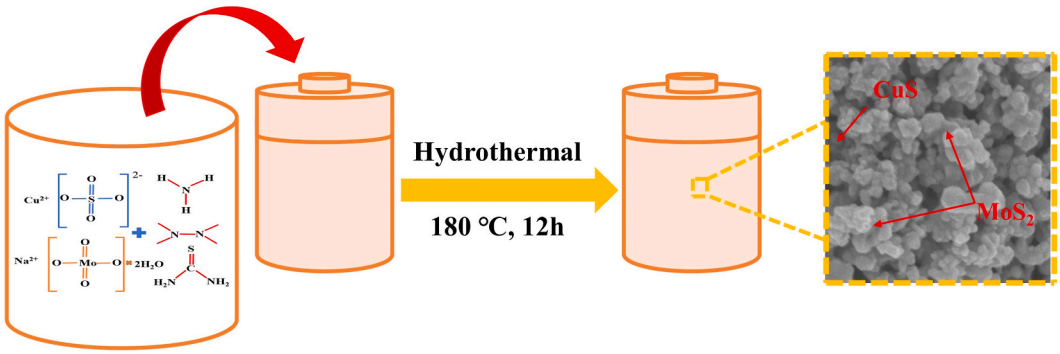

Fig. 1. Scheme showing hydrothermal process for CuS and CuS/MoS_2 synthesis.

metals or metal oxides/sulfide [14–16] instead of enzymes may be the one solution that helps to improve their stability and electrochemical properties. Among these, nanocomposites employing copper in different forms, such as Cu, CuO, Cu_2O, $Cu(OH)_2$, and CuS, exhibit interesting redox properties due to their Cu^{2+}/Cu^{3+}redox pairs that contribute to electrochemical glucose oxidation [17–21]. However, electrochemical glucose oxidation is significantly dependent on the morphology and surface area. Binary copper sulfides occur in two structural forms, CuS (Covellite) and Cu_2S (Chalcocite) [22]. Copper chalcogenides are cost-effective materials that show tunable surface morphology with changes in parameters such as temperature, time, reactant, and reducing agent concentration [23, 24]. This morphology tuning results in excellent optical, electronic, electrochemical, and other physical properties that make the copper chalcogenides-based materials applicable to the Li-ion batteries [25], photocatalysts [26], solar cells [27], supercapacitors [28] and sensors [21]. Despite these benefits, low electron transfer, as well as poor electrical conductivity and dispersion, significantly diminish its effective catalytic activity [29]. To overcome this problem, researchers have prepared composite materials with a carbon-based component [3], including graphene [23], MXene [30], and molybdenum disulfide (MoS_2) [31]. The resulting materials feature increased conductivity as well as surface area of composite material, which play a vital role in the better electrocatalytic activity of electrocatalysts [32].

Molybdenum disulfide (MoS_2), a 2-D transition metal dichalcogenide with a typical band gap of 1.8 eV, exhibits a large surface area, low friction coefficient, better catalytic and physiochemical properties [33–35]. As a graphene analog, MoS_2 may be a viable electrode material for the electrochemical sensors. However, agglomeration, intrinsically low catalytic activity, and low conductivity have so far prevented its broad application [31,36]. So that researchers have attempted to overcome these problems by altering the surface morphology of MoS_2, combining it with supportive functional materials based on carbonaceous materials, conducting polymers, and metals/metal oxides/sulfides nanoparticles resulting in a unique structure and better catalytic properties in the composite material [31,37–39]. Based on this assumption, we used a one-step hydrothermal technique for the first time to prepare a bimetallic CuS/MoS_2 composite for a non-enzymatic electrochemical glucose sensor. The CuS/MoS_2 greatly enhanced the electrocatalytic properties improving ionic mobility, because of synergetic catalytic properties.

2. Materials and methods

The synthesis methods, chemicals used, characterization employed, electrode fabrication, and electrochemical measurement were explained in the supporting information (SI) of the manuscript. The preparation method involved is represented in Fig. 1.

3. Results and discussion

The CuS/MoS_2 composite material synthesis procedure involves the ammonia solution, copper sulfate (copper source), sodium molybdate dihydrate (molybdenum source), thiourea (sulfur source), and hydrazine hydrate (reducing agent), where the hydrazine reduces different metal cations (M^{m+}) to the elemental state (M^0), that undergoes self-oxidation/reduction reaction both in acidic and basic medium as represented in Fig. 1 scheme. Simultaneously, ammonia reacts with copper to form a copper ammonia complex from a complex formation reaction [40]. The reaction can be summarized as,

According to Lee, 1996. [41],

$$M^{m+} + N_2H_4 \rightarrow M^0 \downarrow + N_2 + H^+$$

Based on Tobe and Burgess 1999. [42] discussion, the reduction reaction follows;

$$M^{m+} + N_2H_4 + OH^- \rightarrow M^0 \downarrow + N_2 + NH_3 + H_2O$$

Similarly,

According to Audrieth and Ogg, 1951. [43], hydrazine reacts with dissolved oxygen in the water;

$$N_2H_4 + O_2 \rightarrow N_2 + 2H_2O$$

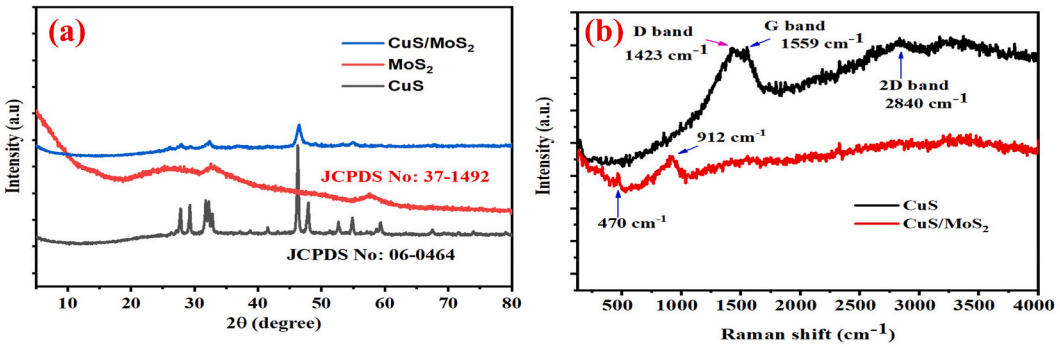

Fig. 2. XRD patterns (a), and Raman spectra (b) of CuS, and CuS/MoS_2.

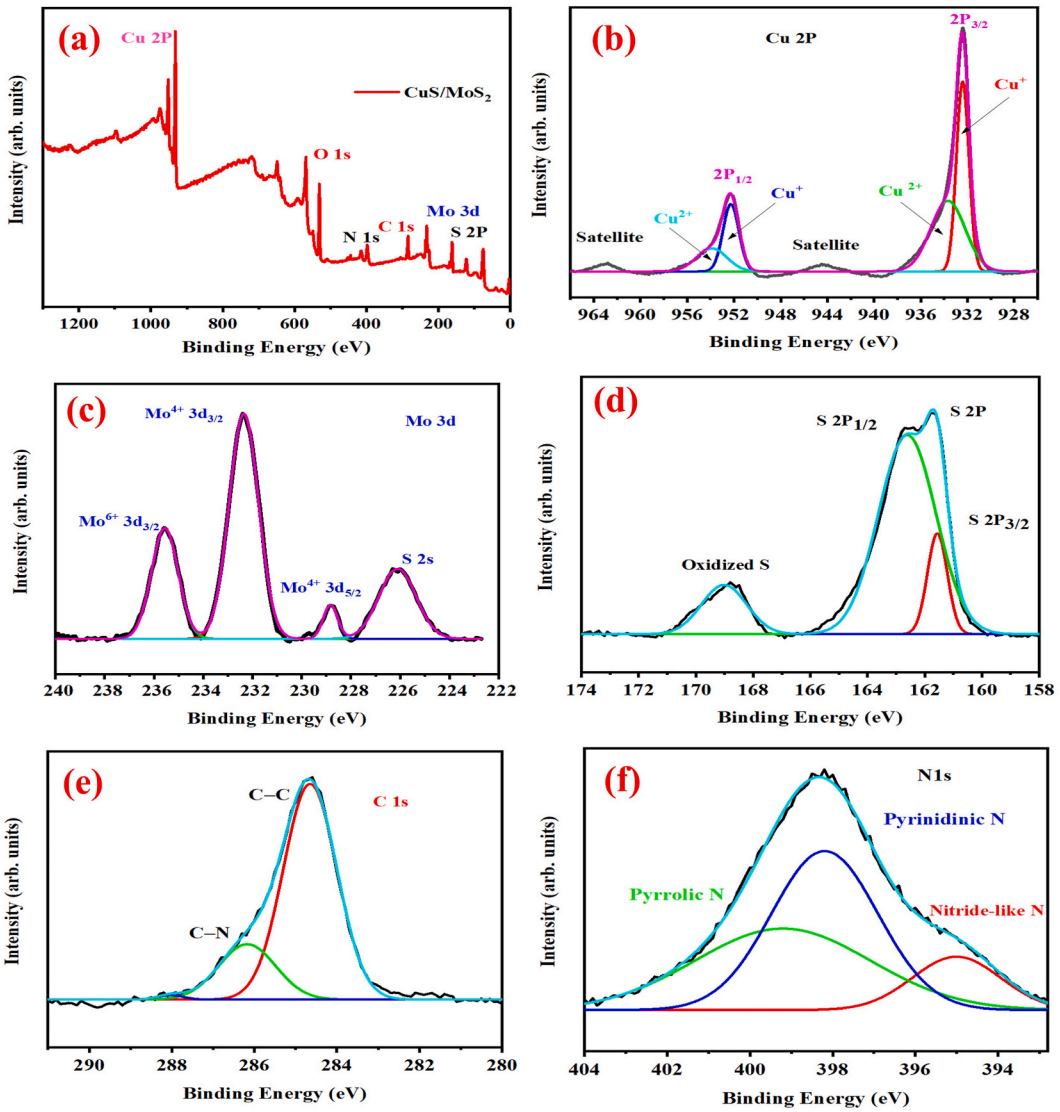

Fig. 3. (a) XPS survey spectrum, (b) Cu 2 P, (c) Mo 3 d, (d) S 2 P, (e) C 1s, and (f) N1s high-resolution XPS spectra.

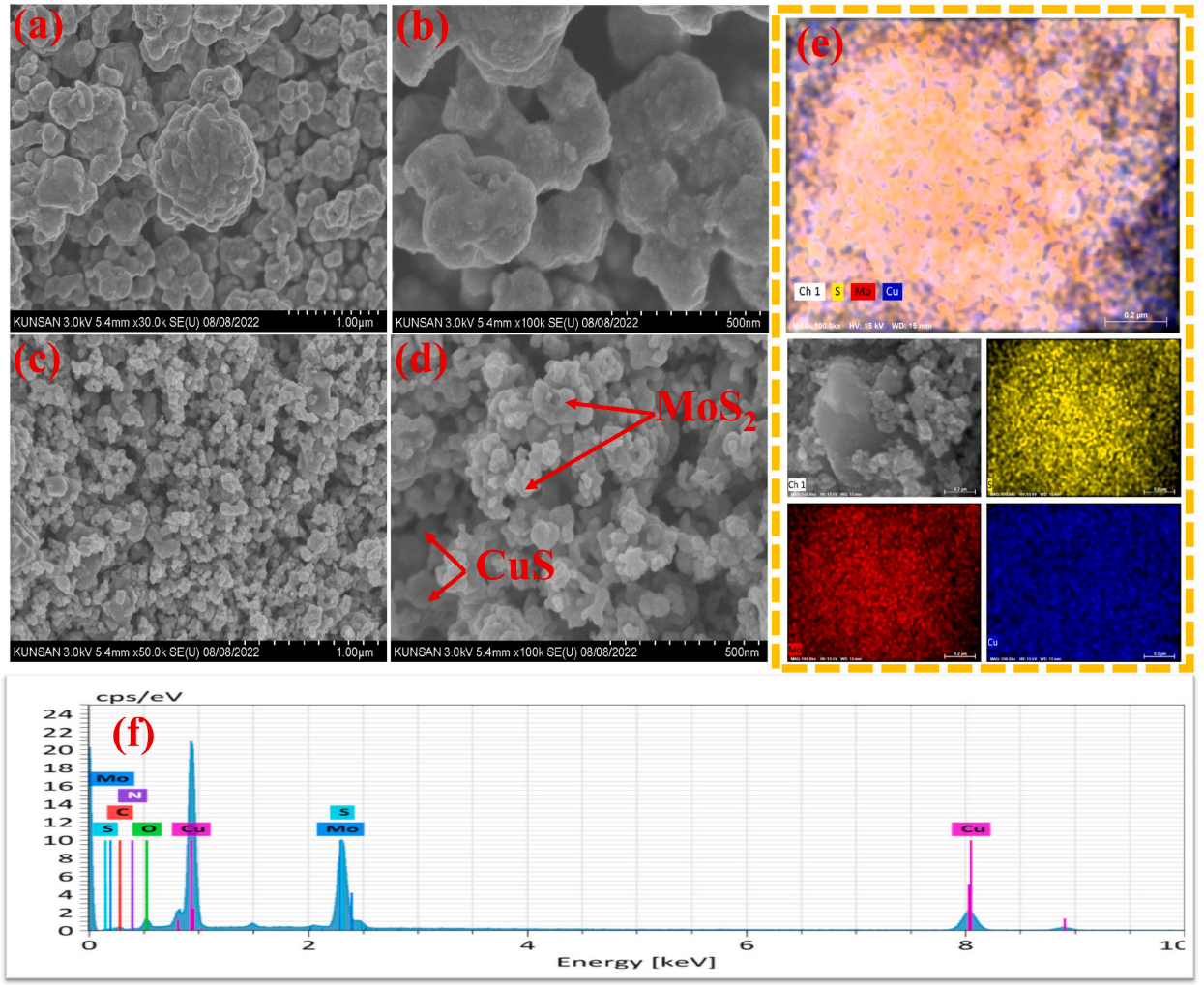

Fig. 4. (a, b) CuS, and (c, d) CuS/MoS_2 FE-SEM images, (e) corresponding EDX mapping, and (f) EDX spectrum of CuS/MoS_2.

The half-reaction involved in the reduction reaction involving hydrazine is as follows [44];

$$N_2H_4 + 2OH^- \rightarrow N_2 + 4H_2O + 4e^- \qquad E^0 = 1.17\ V$$

The reaction between the Cu^{2+} ion and hydrazine can be summarized as,

$$2Cu^{2+} + N_2H_4 \rightarrow 2Cu \downarrow + N_2 + 4\ H^+$$

$$Cu^{2+} + 2N_2H_4 + 2OH^- \rightarrow Cu \downarrow + N_2 + 2NH_3 + 2H_2O$$

The possible mechanism for the copper sulfide assumes that the Cu^{2+} reacts with the S^{2-} ions produced by the hydrolysis of copper salt and thiourea which undergoes a sulfurization reaction during the hydrothermal reaction. The reaction mechanism of CuS and MoS_2 can be described as follows [45,46].

$$Cu^{2+} + 4NH_3 \rightleftharpoons Cu\ (NH_3)_4^{2+}$$

$$NH_3 + H_2O \rightleftharpoons NH_4^+ + OH^-$$

$$(NH_2)_2CS + 2OH \rightleftharpoons S^{2-} + 2H_2O + H_2CN_2$$

$$Cu^{2+} + S^{2-} \rightarrow CuS \downarrow$$

The reaction of sodium molybdate and thiourea in an aqueous medium can be summarized as,

$$4Na_2MoO_4 + 15(NH_2)_2CS + 6H_2O \rightarrow 4MoS_2 \downarrow + Na_2SO_4 + 6NaSCN + 24NH_3 + 9CO_2$$

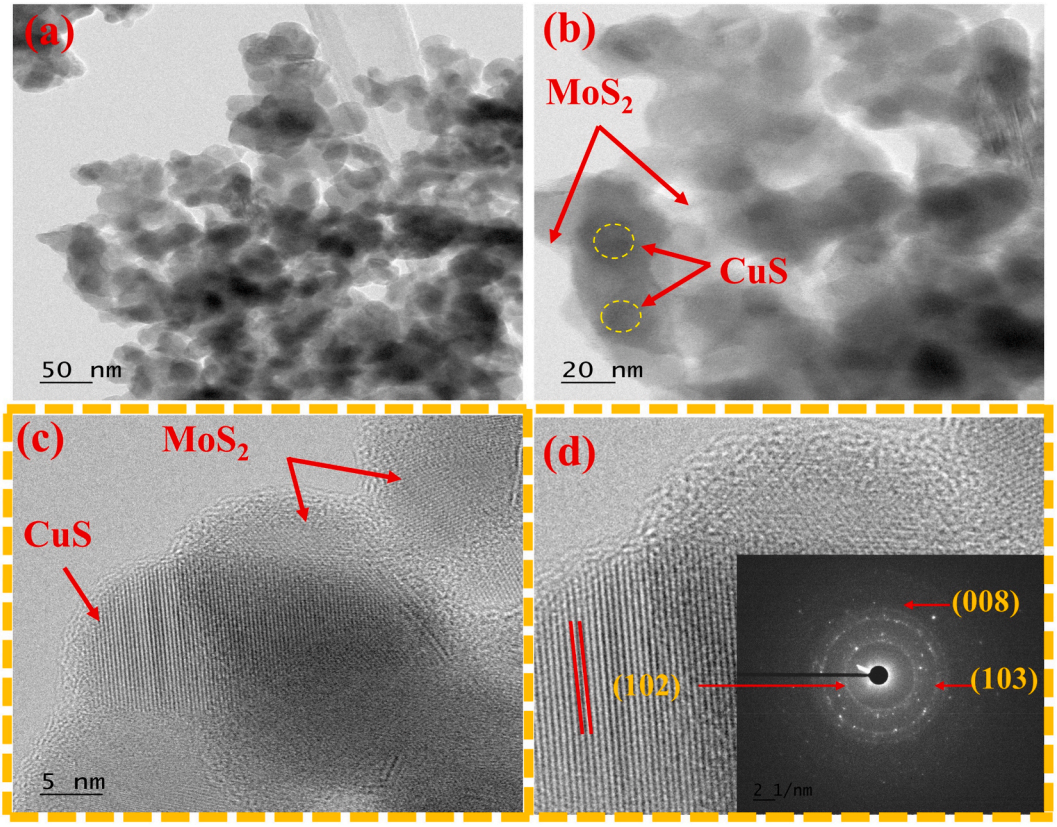

Fig. 5. TEM images (a, b), HR-TEM image (c), and magnified HR-TEM image with d-spacing and SEAD pattern (d) of CuS/MoS_2.

The crystalline phase structure of the composite was characterized by XRD, as illustrated in Fig. 2 (a). The XRD patterns with angle 2θ and crystal planes of the CuS were - 27.84° (101), 29.33° (102), 32.32° (103), 46.28° (008), 47.9° (110), 52.65° (108), 54.92° (104), 59.37° (203), 67.48° (203), 71.72° (207), 74.01° (208). This result resembles prior reported literature (JCPDS No. 06–0464) [3,47,48]. Furthermore, MoS_2 with angle 2θ and corresponding crystal planes: 32.71° (101) and 57.64° (004) shows aquite close accordance with the reported JCPDS No. 37–1492 file [49–51]. The decrease in crystallinity of CuS/MoS_2 composite that possesses a combined peak of CuS and MoS_2 may be accounted for by the dispersion of the MoS_2 nanosheet over the CuS nanostructure, which may have occurred as a result of the combined activity of the hydrazine (reducing agent) and ammonia (complexing agent) [40,52,53]. Raman spectrum of CuS with peaks at 470 cm^{-1} and 912 cm^{-1} corresponds to the S–S stretching and C– N linkage between thiourea and ammonia, respectively, as indicated in Fig. 2(b) [53–59]. Similarly, the peaks indicating D band (1423 cm^{-1}), G band (1559 cm^{-1}), and 2D (2840 cm^{-1}) band highlights the presence of a carbon structure in the CuS [60–63] and the emergence of new bond confirms the creation of a bimetallic sulfide CuS/MoS_2 composite.

The XPS spectrum of the CuS/MoS_2 composite reveals the elemental composition and binding energies as represented in Fig. 3(a). XPS spectrum of CuS/MoS_2 reflects the atomic intensity of Cu, Mo, S, C, and N [3,64,65]. Fig. 3 (b) depicts the deconvolution peaks at 932.34 eV and 952.25 eV binding energies representing the Cu^{+} $2p_{3/2}$ and Cu^{+} $2P_{1/2}$, respectively. Similarly, two more deconvolution peaks at 933.61 eV and 953.87 eV correspond to Cu^{2+} $2P_{3/2}$, and Cu^{2+} $2P_{1/2}$ respectively. Furthermore, satellite peaks at 944.44 eV and 962.84 eV correspond to the paramagnetic chemical state of the Cu^{2+} [66–70]. As shown in Fig. 3 (c), the characteristics peaks at 235.5 eV, 232.3 eV, 288.8 eV, and 226.1 eV indicate the predominance of, Mo^{6+} $3d_{3/2}$, Mo^{4+} 3 $d_{3/2}$, Mo^{4+} $3d_{5/2}$, and S 2s, respectively [31,71–73]. The peaks represented in Fig. 3 (d), specify deconvolution peaks situated at 161.5 eV, 162.5 eV, and 168.9 eV indicating S $2P_{3/2}$, S $2P_{1/2}$, and oxidized S respectively [3,74–77]. Fig. 3 (e) represents fitted peaks at 284.6 eV and 286.1 eV assigned to C–C and C–N, respectively [3,65,78,79]. As represented in Fig. 3 (f), peaks at 394.9 eV, 298.1 eV, and 299.3 eV, correspond to nitride-like- N, pyridinic-N, and pyrrolic-N, respectively [65,80–83].

Surface morphology was characterized by using FE-SEM (in Fig. 4), and HRTEM (Fig. 5) [84]. The FE-SEM images of CuS at 30 K and 100 K magnification revealed its aggregated ball-like nanostructures (Fig. 4 (a, b)) [85]. Furthermore, the FE-SEM image of CuS/MoS_2 indicates the MoS_2 nanosheet grown at the CuS surface (Fig. 4 (c, d)) [85]. The surface morphology modification after synergy between CuS and 2-D MoS_2 decreases agglomeration and increases sufficient electrochemically active sites by increasing surface area resulting in better electrocatalytic activity [86,87]. As shown in Fig. 4. (d), the FE-SEM image of the CuS/MoS_2 composite reflects a clear surface morphology with two different components (CuS and MoS_2). The EDX color mapping of CuS/MoS_2 composite (Fig. 4. (e)) and EDX spectrum of CuS/MoS_2 composite (Fig. 4. (f)) indicates the presence of CuS and MoS_2 in the CuS/MoS_2 composite

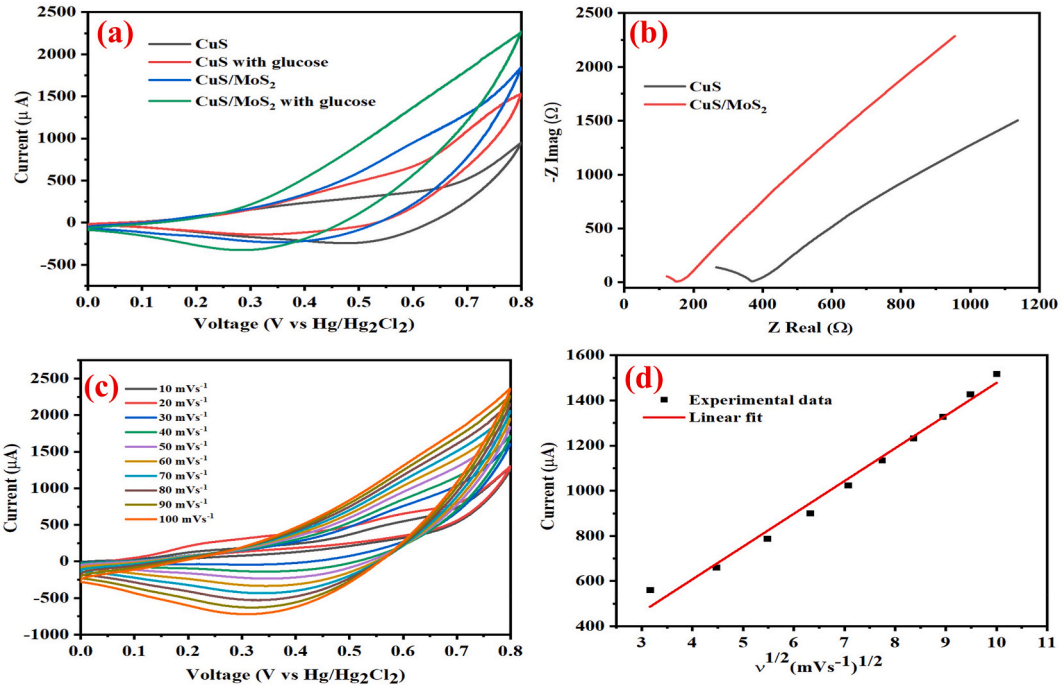

Fig. 6. CV spectra with and without glucose (a), Nyquist plot of CuS and CuS/MoS_2 (b), CV of CuS/MoS_2 at various scan rates (c), linear fit of sq. root of scan rate against oxidation current (d).

material [3,88].

The morphology of the CuS/MoS_2 was analyzed using Cs -STEM micrographs. The result revealed that the CuS was wrapped with dispersed molybdenum nanosheets (Fig. 5. (a, b)). The HR-TEM image of CuS revealed 0.32 nm lattice spacing with crystal plane (102) (Fig. 5 (c and d). The SEAD pattern of CuS/MoS_2 composite indicates polycrystallinity with circular rings that support the crystal planes (102), and (103) and the (008) of CuS (inset image in Fig. 5(d).) [89–91].

3.1. Electrochemical glucose sensing

The electrocatalytic activity of CuS/MoS_2 and CuS were analyzed without and with glucose addition (2 mM) using 0.1 M NaOH electrolyte in a three-electrode system. Herein, we can figure out the gradual current increment in CuS/MoS_2 electrode as compared to the CuS at 50 mVs^{-1} in cyclic voltammetric response shows the improved electrocatalytic activity of the CuS/MoS_2 composite. Similarly, in CuS and CuS/MoS_2 electrode oxidation current increment after the addition of glucose signifies the feasibility of electrode material towards non-enzymatic glucose sensor, as shown in Fig. 6 (a) [3,65,92]. The increased current response is due to the synergy of bimetallic sulfides and increased dispersion due to molybdenum disulfide nanosheets [93]. The HR-TEM image of the CuS/MoS_2 nanostructure indicates the accessible sites that promote electron transfer during the electro-oxidation of glucose [94]. The morphological structure of the CuS/MoS_2 composite suggests that the dispersion of the MoS_2 nanosheet over the CuS nanostructure, which increases potential active site and improves electrolytic dispersion, in turn, enhances electrochemical glucose oxidation through Cu (II/III) mediated electrochemical reversible redox reactions in an alkaline electrolyte, which are as summarized below [3,65,95,96].

$$CuS + 2OH^- \rightarrow Cu(OH)_2 + S + 2e^- \quad (1)$$

$$Cu\,(OH)_2 + OH^- \rightarrow CuOOH + H_2O + e^- \quad (2)$$

$$CuOOH + \text{glucose} \rightarrow Cu\,(OH)_2 + \text{gluconolactone} \quad (3)$$

We performed an EIS analysis of CuS/MoS_2 and CuS electrodes in an equal volume ratio of ferricyanide solution (5 mM) and potassium chloride (0.1 M) solution at 0.1 Hz to 100 kHz frequency as shown in Fig. 6(b). Slope increment of the CuS/MoS_2 in the higher frequency region as compared to CuS suggests better electrocatalytic property of CuS/MoS_2 [85,97], that corresponds to synergetic behavior of the CuS and MoS_2 in CuS/MoS_2 composite [3].

Fig. 6(c) shows a cyclic voltammogram of CuS/MoS_2 composite with current response and scan rate relationship. The increase in anodic oxidation current along with concerning scan rates (10-100 mVs^{-1}) demonstrates the linear dependence [65]. Solving the regression equation obtained from linear regression between oxidation peak current response vs square root of scan rate we get $R^2 = 0.987$, which indicates the potentiality for the diffusion-controlled electrochemical reaction at the electrode surface of CuS/MoS_2

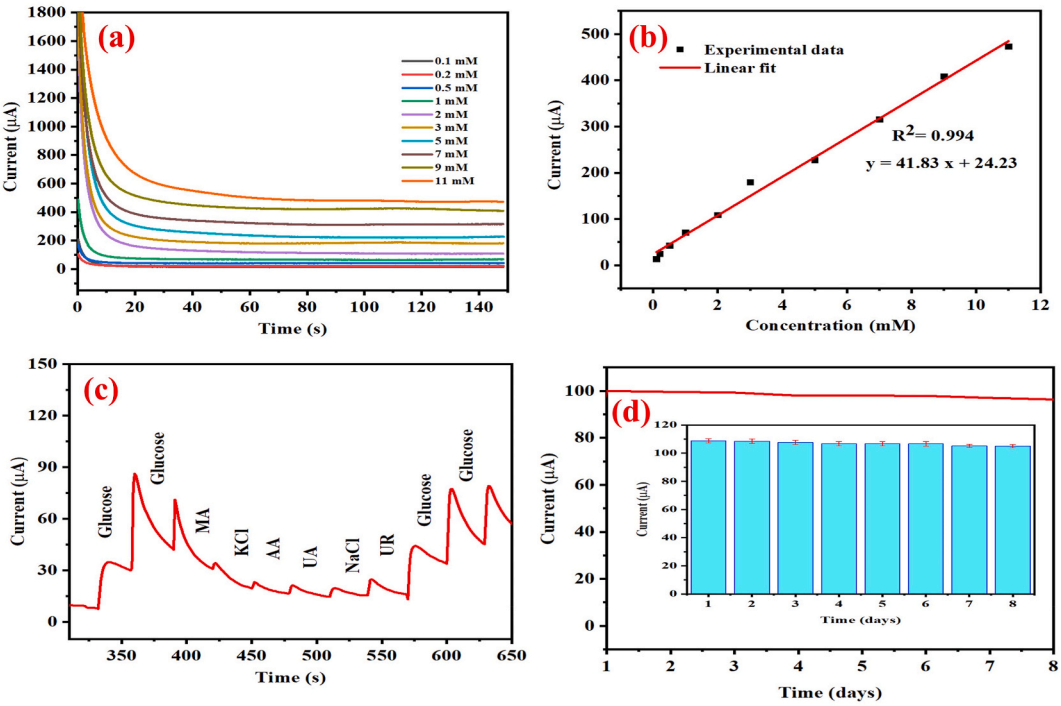

Fig. 7. Chronoamperometry curves of CuS/MoS_2 samples with glucose concentration (100 μM −11 mM) (a), linear fitting of Current Vs. concentration plot of CuS/MoS_2 (b), interference study using glucose and potential interfering species (c) and Stability test of CuS/MoS_2 electrode to 2 mM glucose showing change over time (days) (d).

Table 1
The comparison table of Cu- and Mo-based electrodes for glucose sensing.

Electrode material	Linear range	Detection limit	Sensitivity	Ref.
CuS MF	0.02–5.4 mM	2.0 μM	1007 μA $mM^{-1}cm^{-2}$	[21]
Bilayer MoS_2	30–300 mM	300 nM	260.75 μA $mM^{-1}cm^{-2}$	[99]
MoS_2-CuNPs	4–4000 μM	–	1055 μA $mM^{-1}cm^{-2}$	[100]
MoS_2-CuS	1–100 μM	0.3 μM	–	[101]
CuO/MoS_2	0.1–1 mM	0.017 μM	1055 μA $mM^{-1}cm^{-2}$	[94]
Cu_xS-MoS_2-rGO	2–720 μM	0.6 μM	308.2 μA $mM^{-1}cm^{-2}$	[31]
CuS nanotube	0.05–5 μM	–	7.842 μA $mM^{-1}cm^{-2}$	[102]
Cu–Cu_2S	0.002–8.1 mM	0.1 μM	361.58 μA $mM^{-1}cm^{-2}$	[103]
CuS/MoS_2	0.1–11 mM	1.52 μM	252.71 μA mM^{-1} cm^{-2}	This work

composite. The electron transfer kinetics in electrochemical reaction occurs as a result of charge separation through a diffusion-controlled reaction mediated by charge separation and diffusion process due to MoS_2 nanosheet, which is shown in Fig. 6(d) [65,85,94].

3.2. Chronoamperometric analysis

The chronoamperometric spectra of CuS/MoS_2 are represented in Fig. 7(a) [3,85]. The result depicts that the gradual addition of glucose in the concentration range (100 μM- 11 mM) into an alkaline medium solution gives rise to the current increment. This result supports the idea that this material may have a practical application as an electrode material capable of monitoring glucose levels at 0.5 V applied potential. On plotting the oxidation current against the concentration, we get a linear fitting with R^2 value of 0.994, as shown in Fig. 7(b) [3]. The sensitivity of the CuS/MoS_2 electrode-based glucose sensor was estimated using $S = m/A$, in which m and A respectively represent the slope obtained from the calibration plot and the electrochemical active surface area (A = 0.1655 cm^2) of the electrode. The limit of the detection LOD was calculated using the formula; LOD = $3\sigma/m$, (where, σ = standard derivation, and m = slope) [3,85,94,95,98]. The sensitivity and detection limit were found to be 252.71 μA mM^{-1} cm^{-2} and 1.52 μM, respectively. Table 1 compares linear range, detection limit and sensitivity of related materials developed and described by elsewhere.

Table 2
Determination of glucose in diluted human serum.

Sample	Added glucose concentration (μM)	Found glucose concentration (μM)	Recovery (%)	RSD (%)
1	500	483	96.60	1.29
2	1000	969	96.90	1.00
3	2000	1966	98.30	1.10

3.3. Selectivity and stability analysis

To prove the better selectivity a sensor should be able to detect interfering reagent species along with glucose during electrochemical reaction in chronoamperometry analysis. For that, the selectivity of CuS/MoS_2 electrode-based glucose sensor was checked by subjecting glucose solution (1.0 mM) as well as interfering reagent solutions such as ascorbic acid (AA), maleic acid (MA), potassium chloride (KCl), urea (UR), uric acid (UA), and sodium chloride (NaCl), (0.5 mM) [3,70]. The simultaneous oxidation of interfering agents and glucose during an electrochemical reaction demonstrates the selectivity of the CuS/MoS_2 as shown in Fig. 7(c) [3,85]. The selectivity of the CuS/MoS_2 electrode over potential interring reagents is proved by the relatively low current response as compared to the glucose in an electrochemical reaction [3]. The stability was estimated by chronoamperometric tests over eight days. The sensitivity of CuS/MoS_2 was found to have decreased by 3.26 % over that time, showing 96.47 % stability (Fig. 7(d)). This reproducibility is thus quite adequate for an electrode material.

3.4. Real sample analysis

For the real sample analysis, a standard addition method was used to measure the recovery percentage by putting glucose solution of known concentration into diluted normal human serum (H4522, Sigma-Aldrich, 4.89 mM) [3] sample in alkaline medium. As tabulated in Table 2 the CuS/MoS_2 based electrode demonstrated a recovery percentage of 96.60 %, 96.90 % and 98.30 %, in response for the 500 μM, 1000 μM, and 2000 μM concentration of glucose solution [85]. These results suggest that the CuS/MoS_2 based electrode is viable for non-enzymatic glucose sensor as proven by a relative standard deviation (RSD) of less than 1.3 % [3,65,104].

4. Conclusions

We synthesized CuS/MoS_2 through one-step hydrothermal method. The structural morphology of the nanocomposite was characterized using diverse techniques to assess its suitability for the electrochemical non-enzymatic glucose sensor. The morphological structure of the CuS/MoS_2 provides an active site for glucose electrooxidation. The composite exhibits a sensitivity of 252.71 μA mM^{-1} cm^{-2}, a linear rang 100 μM-11 mM, and a detection limit of 1.52 μM. The CuS/MoS_2-based glucose sensor's remarkable selectivity towards interfering species, as well as its stability, suggest that it has potential as a non-enzymatic electrochemical glucose sensor.

Data availability statement

Data will be made available on request.

CRediT authorship contribution statement

Krishna Prasad Sharma: Writing – original draft, Visualization, Validation, Methodology, Investigation, Formal analysis, Data curation, Conceptualization. **Miyeon Shin:** Writing – review & editing, Software, Resources, Project administration, Data curation. **Ganesh Prasad Awasthi:** Software, Project administration, Methodology, Funding acquisition. **Soonhwan Cho:** Visualization, Software, Resources, Project administration, Methodology, Funding acquisition. **Changho Yu:** Writing – review & editing, Supervision, Project administration, Investigation, Funding acquisition, Formal analysis.

Declaration of competing interest

The authors declare that they have no known competing financial interests or personal relationships that could have appeared to influence the work reported in this paper.

Acknowledgement

This research was supported by Korean Institute of Marine Science & Technology Promotion (KIMST) funded by the Ministry of Oceans and Fisheries, Korea (20220583), and this work was also supported by a grant from the National Research Foundation of Korea (NRF) funded by the Korea government (MSIT) (project no. NRF-2022R1A2C1093320) and supported by "Research Base Construction Fund Support Program" funded by Jeonbuk National University in 2023. We are also grateful to the Center for University-wide Research Facilities (CURF) at Jeonbuk National University for their assistance is providing the equipment necessary to perform our tests. We would also like to express our gratitude to the editors at Jeonbuk National University's Writing Center for their English

language assistance.

Appendix A. Supplementary data

Supplementary data to this article can be found online at https://doi.org/10.1016/j.heliyon.2023.e23721.

References

[1] D.-Y. Lu, J.-Y. Che, N.S. Yarla, H.-Y. Wu, T.-R. Lu, B. Xu, S.-Y. Wu, J. Ding, Y. Lu, H. Zhu, Type 2 diabetes treatment and drug development study, Open Diabetes J. 8 (2018).
[2] N.N. Tun, G. Arunagirinathan, S.K. Munshi, J.M. Pappachan, Diabetes mellitus and stroke: a clinical update, World J. Diabetes 8 (2017) 235.
[3] K.P. Sharma, M. Shin, G.P. Awasthi, M.B. Poudel, H.J. Kim, C. Yu, Chitosan polymer matrix-derived nanocomposite (CuS/NSC) for non-enzymatic electrochemical glucose sensor, Int. J. Biol. Macromol. 206 (2022) 708–717.
[4] K. Dhara, D.R. Mahapatra, Electrochemical nonenzymatic sensing of glucose using advanced nanomaterials, Microchim. Acta 185 (2017) 49.
[5] W.H. Organization, World Health Statistics Overview 2019: Monitoring Health for the SDGs, Sustainable Development Goals, World Health Organization, 2019.
[6] S. Chen, X. Hai, X.-W. Chen, J.-H. Wang, In situ growth of silver nanoparticles on graphene quantum dots for ultrasensitive colorimetric detection of H2O2 and glucose, Anal. Chem. 86 (2014) 6689–6694.
[7] T. Meng, N. Shang, J. Zhao, M. Su, C. Wang, Y. Zhang, Facile one-pot synthesis of Co coordination polymer spheres doped macroporous carbon and its application for electrocatalytic oxidation of glucose, J. Colloid Interface Sci. 589 (2021) 135–146.
[8] R. Wilson, A.P.F. Turner, Glucose oxidase: an ideal enzyme, Biosens. Bioelectron. 7 (1992) 165–185.
[9] A. Esmaeeli, A. Ghaffarinejad, A. Zahedi, O. Vahidi, Copper oxide-polyaniline nanofiber modified fluorine doped tin oxide (FTO) electrode as non-enzymatic glucose sensor, Sensor. Actuator. B Chem. 266 (2018) 294–301.
[10] H. Zheng, M. Liu, Z. Yan, J. Chen, Highly selective and stable glucose biosensor based on incorporation of platinum nanoparticles into polyaniline-montmorillonite hybrid composites, Microchem. J. 152 (2020), 104266.
[11] F. Bettazzi, C. Ingrosso, P.S. Sfragano, V. Pifferi, L. Falciola, M.L. Curri, I. Palchetti, Gold nanoparticles modified graphene platforms for highly sensitive electrochemical detection of vitamin C in infant food and formulae, Food Chem. 344 (2021), 128692.
[12] M. Baghayeri, A. Amiri, S. Farhadi, Development of non-enzymatic glucose sensor based on efficient loading Ag nanoparticles on functionalized carbon nanotubes, Sensor. Actuator. B Chem. 225 (2016) 354–362.
[13] Q. Xu, Y. Zhao, J.Z. Xu, J.-J. Zhu, Preparation of functionalized copper nanoparticles and fabrication of a glucose sensor, Sensor. Actuator. B Chem. 114 (2006) 379–386.
[14] K.-Y. Hwa, B. Subramani, Synthesis of zinc oxide nanoparticles on graphene–carbon nanotube hybrid for glucose biosensor applications, Biosens. Bioelectron. 62 (2014) 127–133.
[15] J. Zhang, X. Xiao, Q. He, L. Huang, S. Li, F. Wang, A nonenzymatic glucose sensor based on a copper nanoparticle–zinc oxide nanorod array, Anal. Lett. 47 (2014) 1147–1161.
[16] C. Karuppiah, M. Velmurugan, S.-M. Chen, S.-H. Tsai, B.-S. Lou, M.A. Ali, F.M.A. Al-Hemaid, A simple hydrothermal synthesis and fabrication of zinc oxide–copper oxide heterostructure for the sensitive determination of nonenzymatic glucose biosensor, Sensor. Actuator. B Chem. 221 (2015) 1299–1306.
[17] Y. Zhang, N. Li, Y. Xiang, D. Wang, P. Zhang, Y. Wang, S. Lu, R. Xu, J. Zhao, A flexible non-enzymatic glucose sensor based on copper nanoparticles anchored on laser-induced graphene, Carbon 156 (2020) 506–513.
[18] S.A. Khayyat, S.G. Ansari, A. Umar, Glucose sensor based on copper oxide nanostructures, J. Nanosci. Nanotechnol. 14 (2014) 3569–3574.
[19] A. Jiménez-Rodríguez, E. Sotelo, L. Martínez, Y. Huttel, M.U. González, A. Mayoral, J.M. García-Martín, M. Videa, J.L. Cholula-Díaz, Green synthesis of starch-capped Cu2O nanocubes and their application in the direct electrochemical detection of glucose, RSC Adv. 11 (2021) 13711–13721.
[20] Y.J. Yang, W. Li, X. Chen, Highly enhanced electrocatalytic oxidation of glucose on Cu (OH) 2/CuO nanotube arrays modified copper electrode, J. Solid State Electrochem. 16 (2012) 2877–2881.
[21] S. Radhakrishnan, H.-Y. Kim, B.-S. Kim, A novel CuS microflower superstructure based sensitive and selective nonenzymatic glucose detection, Sensor. Actuator. B Chem. 233 (2016) 93–99.
[22] U. Shamraiz, R.A. Hussain, A. Badshah, Fabrication and applications of copper sulfide (CuS) nanostructures, J. Solid State Chem. 238 (2016) 25–40.
[23] X. Yan, Y. Gu, C. Li, B. Zheng, Y. Li, T. Zhang, Z. Zhang, M. Yang, Non-enzymatic glucose sensor based on the CuS nanoflakes-reduced graphene oxide nanocomposite, Anal. Methods 10 (2017).
[24] Y.J. Yang, J. Zi, W. Li, Enzyme-free sensing of hydrogen peroxide and glucose at a CuS nanoflowers modified glassy carbon electrode, Electrochim. Acta 115 (2014) 126–130.
[25] G. Kalimuldina, A. Nurpeissova, A. Adylkhanova, N. Issatayev, D. Adair, Z. Bakenov, 3D hierarchical nanocrystalline CuS cathode for lithium batteries, Materials 14 (2021) 1615.
[26] G. Nabi, M. Tanveer, M. Bilal Tahir, M. Kiran, M. Rafique, N.R. Khalid, M. Alzaid, N. Fatima, T. Nawaz, Mixed solvent based surface modification of CuS nanostructures for an excellent photocatalytic application, Inorg. Chem. Commun. 121 (2020), 108205.
[27] M.A. Sangamesha, K. Pushpalatha, G.L. Shekar, S. Shamsundar, Preparation and characterization of nanocrystalline CuS thin films for dye-sensitized solar cells, ISRN Nanomaterials 2013 (2013), 829430.
[28] H. Peng, G. Ma, K. Sun, J. Mu, H. Wang, Z. Lei, High-performance supercapacitor based on multi-structural CuS@polypyrrole composites prepared by in situ oxidative polymerization, J. Mater. Chem. A 2 (2014) 3303–3307.
[29] M. Keerthi, B. Mutharani, S.M. Chen, P. Ranganathan, Carbon fibers coated with urchin-like copper sulfide for nonenzymatic voltammetric sensing of glucose, Mikrochim. Acta 186 (2019) 807.
[30] Y. Li, Z. Kang, L. Kong, H. Shi, Y. Zhang, M. Cui, D.-P. Yang, MXene-Ti3C2/CuS nanocomposites: enhanced peroxidase-like activity and sensitive colorimetric cholesterol detection, Mater. Sci. Eng. C 104 (2019), 110000.
[31] F. Xu, M. Wu, G. Ma, H. Xu, W. Shang, Copper-molybdenum sulfide/reduced graphene oxide hybrid with three-dimensional wrinkles and pores for enhanced amperometric detection of glucose, Microchem. J. 159 (2020), 105432.
[32] I.-H. Cho, D.H. Kim, S. Park, Electrochemical biosensors: perspective on functional nanomaterials for on-site analysis, Biomater. Res. 24 (2020) 6.
[33] X. Li, H. Zhu, Two-dimensional MoS2: properties, preparation, and applications, Journal of Materiomics 1 (2015) 33–44.
[34] J.A. Wilson, A.D. Yoffe, The transition metal dichalcogenides discussion and interpretation of the observed optical, electrical and structural properties, Adv. Phys. 18 (1969) 193–335.
[35] I. Rahman, A. Purqon, First principles study of molybdenum disulfide electronic structure, J. Phys. Conf. 877 (2017), 012026.
[36] N.A. Kumar, M.A. Dar, R. Gul, J.-B. Baek, Graphene and molybdenum disulfide hybrids: synthesis and applications, Mater. Today 18 (2015) 286–298.
[37] X. Sui, L. Zhang, J. Li, K. Doyle-Davis, R. Li, Z. Wang, X. Sun, Advanced support materials and interactions for atomically dispersed noble-metal catalysts: from support effects to design strategies, Adv. Energy Mater. 12 (2022), 2102556.

[38] F. Guo, H. Yang, L. Liu, Y. Han, A.M. Al-Enizi, A. Nafady, P.E. Kruger, S.G. Telfer, S. Ma, Hollow capsules of doped carbon incorporating metal@metal sulfide and metal@metal oxide core–shell nanoparticles derived from metal–organic framework composites for efficient oxygen electrocatalysis, J. Mater. Chem. A 7 (2019) 3624–3631.
[39] H. Zengin, G. Kalaycı, Synthesis and characterization of polyaniline/activated carbon composites and preparation of conductive films, Mater. Chem. Phys. 120 (2010) 46–53.
[40] S.K. Haram, A.R. Mahadeshwar, S.G. Dixit, Synthesis and characterization of copper sulfide nanoparticles in triton-X 100 water-in-oil microemulsions, J. Phys. Chem. 100 (1996) 5868–5873.
[41] J.D. Lee, Concise Inorganic Chemistry, John Wiley & Sons, 2008.
[42] M.L. Tobe, J. Burgess, Inorganic Reaction Mechanisms, Longman, 1999.
[43] L.F. Audrieth, B.A. Ogg, B. Ackerson, The Chemistry of Hydrazine, Wiley, 1951.
[44] J.P. Chen, L.L. Lim, Key factors in chemical reduction by hydrazine for recovery of precious metals, Chemosphere 49 (2002) 363–370.
[45] S. Haram, R. Mahadeshwar, S. Dixit, Synthesis and characterization of copper sulphide nanoparticles in aqueous surfactant solutions, Adsorpt. Sci. Technol. 16 (1998) 667–677.
[46] S. Wang, G. Li, G. Du, X. Jiang, C. Feng, Z. Guo, S.-J. Kim, Hydrothermal synthesis of molybdenum disulfide for lithium ion battery applications, Chin. J. Chem. Eng. 18 (2010) 910–913.
[47] H. Lee, S.W. Yoon, E.J. Kim, J. Park, In-situ growth of copper sulfide nanocrystals on multiwalled carbon nanotubes and their application as novel solar cell and amperometric glucose sensor materials, Nano Lett. 7 (2007) 778–784.
[48] C. Wei, X. Zou, Q. Liu, S. Li, C. Kang, W. Xiang, A highly sensitive non-enzymatic glucose sensor based on CuS nanosheets modified Cu2O/CuO nanowire arrays, Electrochim. Acta 334 (2020), 135630.
[49] M. Sookhakian, W.J. Basirun, B.T. Goh, P.M. Woi, Y. Alias, Molybdenum disulfide nanosheet decorated with silver nanoparticles for selective detection of dopamine, Colloids Surf. B Biointerfaces 176 (2019) 80–86.
[50] C.P. Veeramalai, F. Li, Y. Liu, Z. Xu, T. Guo, T.W. Kim, Enhanced field emission properties of molybdenum disulphide few layer nanosheets synthesized by hydrothermal method, Appl. Surf. Sci. 389 (2016) 1017–1022.
[51] Y. Hou, Y. Ren, S. Zhang, K. Wang, F. Yu, T. Zhu, 3D S@MoS2@reduced graphene oxide aerogels cathode for high-rate lithium-sulfur batteries, J. Alloys Compd. 852 (2021), 157011.
[52] N. Meng, Y. Zhou, W. Nie, L. Song, P. Chen, CuS/MoS2 nanocomposite with high solar photocatalytic activity, J. Nanoparticle Res. 17 (2015) 300.
[53] Y. Zhu, Y. Lu, S.H. Sun, B. Zhou, Y.M. Hu, Phase selectivity of copper sulfide: synthesis and application, J. Electron. Mater. 50 (2021) 2034–2042.
[54] T. Zhao, X. Peng, X. Zhao, J. Hu, T. Jiang, X. Lu, H. Zhang, T. Li, I. Ahmad, Preparation and performance of carbon dot decorated copper sulphide/carbon nanotubes hybrid composite as supercapacitor electrode materials, J. Alloys Compd. 817 (2020), 153057.
[55] T. Hurma, S. Kose, XRD Raman analysis and optical properties of CuS nanostructured film, Optik 127 (2016) 6000–6006.
[56] A.G. Milekhin, N.A. Yeryukov, L.L. Sveshnikova, T.A. Duda, E.E. Rodyakina, V.A. Gridchin, E.S. Sheremet, D.R.T. Zahn, Combination of surface-and interference-enhanced Raman scattering by CuS nanocrystals on nanopatterned Au structures, Beilstein J. Nanotechnol. 6 (2015) 749–754.
[57] N.A. Yeryukov, A.G. Milekhin, L.L. Sveshnikova, T.A. Duda, L.D. Pokrovsky, A.K. Gutakovskii, S.A. Batsanov, E.E. Rodyakina, A.V. Latyshev, D.R.T. Zahn, Synthesis and characterization of CuxS (x = 1–2) nanocrystals formed by the Langmuir–blodgett technique, J. Phys. Chem. C 118 (2014) 23409–23414.
[58] K. Maslana, R. Kalenczuk, B. Zielińska, E. Mijowska, Synthesis and characterization of nitrogen-doped carbon nanotubes derived from g-C3N4, Materials 13 (2020) 1349.
[59] Q. Zeng, D.-W. Wang, K.-H. Wu, Y. Li, F. Godoi, I. Gentle, Synergy of nanoconfinement and surface oxygen in recrystallization of sulfur melt in carbon nanocapsules and the related Li–S cathode properties, J. Mater. Chem. A 2 (2014).
[60] Y. Lu, X. Liu, W. Wang, J. Cheng, Y. Hailong, C. Tang, J.-K. Kim, Y. Luo, Hierarchical, porous CuS microspheres integrated with carbon nanotubes for high-performance supercapacitors, Sci. Rep. 5 (2015), 16584.
[61] C. Sole, N.E. Drewett, L.J. Hardwick, In situ Raman study of lithium-ion intercalation into microcrystalline graphite, Faraday Discuss 172 (2014) 223–237.
[62] N. Karikalan, R. Karthik, S.-M. Chen, C. Karuppiah, A. Elangovan, Sonochemical synthesis of sulfur doped reduced graphene oxide supported CuS nanoparticles for the non-enzymatic glucose sensor applications, Sci. Rep. 7 (2017).
[63] A. Ray, S. Chatterjee, J. Singh, H. Bapari, Thermal exfoliation of natural cellulosic material for graphene synthesis, J. Mater. Eng. Perform. (2015) 24.
[64] J. Li, Q. Wu, X. Wang, B. Wang, T. Liu, Metal-organic framework-derived Co/CoO nanoparticles with tunable particle size for strong low-frequency microwave absorption in the S and C bands, J. Colloid Interface Sci. 628 (2022) 10–21.
[65] K.P. Sharma, M. Shin, G.P. Awasthi, C. Yu, One-pot hydrothermal synthesis of CuS/CoS composite for electrochemical non-enzymatic glucose sensor, Curr. Appl. Phys. 56 (2023) 126–134.
[66] Z. Yu, F. Li, H. Di, Y. Pan, L. Lv, Y. Ma, Q. Chen, A facile one-pot method for preparation of the rGO–CuS/Cu2S with enhanced photocatalytic activity under visible light irradiation, J. Mater. Sci. Mater. Electron. 27 (2016) 5136–5144.
[67] S. Adhikari, D. Sarkar, G. Madras, Hierarchical design of CuS architectures for visible light photocatalysis of 4-chlorophenol, ACS Omega 2 (2017) 4009–4021.
[68] H. Liu, Z. Guo, X. Wang, J. Hao, J. Lian, CuS/MnS composite hexagonal nanosheet clusters: synthesis and enhanced pseudocapacitive properties, Electrochim. Acta 271 (2018) 425–432.
[69] H. Luo, H. Lei, Y. Yuan, Y. Liang, Y. Qiu, Z. Zhu, Z. Wang, Engineering ternary copper-cobalt sulfide nanosheets as high-performance electrocatalysts toward oxygen evolution reaction, Catalysts (2019).
[70] J. Lv, C. Kong, Y. Xu, Z. Yang, X. Zhang, S. Yang, G. Meng, J. Bi, J. Li, S. Yang, Facile synthesis of novel CuO/Cu2O nanosheets on copper foil for high sensitive nonenzymatic glucose biosensor, Sensor. Actuator. B Chem. 248 (2017) 630–638.
[71] M.R. Kandel, U.N. Pan, D.R. Paudel, P.P. Dhakal, N.H. Kim, J.H. Lee, Hybridized bimetallic phosphides of Ni–Mo, Co–Mo, and Co–Ni in a single ultrathin-3D-nanosheets for efficient HER and OER in alkaline media, Compos. B Eng. 239 (2022), 109992.
[72] B. Wang, D. Zhang, H. Wang, H. Zhao, R. Liu, Q. Li, S. Zhou, J. Du, Q. Xu, Enhanced room temperature ferromagnetism in MoS 2 by N plasma treatment, AIP Adv. 10 (2020), 015243.
[73] Z. Han, Z. Tang, K. Jiang, Q. Huang, J. Meng, D. Nie, Z. Zhao, Dual-target electrochemical aptasensor based on co-reduced molybdenum disulfide and Au NPs (rMoS2-Au) for multiplex detection of mycotoxins, Biosens. Bioelectron. 150 (2020), 111894.
[74] M. Keerthi, B. Mutharani, S.-M. Chen, P. Ranganathan, Carbon fibers coated with urchin-like copper sulfide for nonenzymatic voltammetric sensing of glucose, Microchim. Acta 186 (2019) 807.
[75] A. Munir, Immobilization of Nanocluster on Functionalized Graphene Oxide for Water OxidationCatalysis, 2019.
[76] Q. Wang, X. Zhao, X. Zhang, Y.-I. Lee, H.-G. Liu, Fabrication of porous thin films of block copolymer at the liquid/liquid interface and construction of composite films doped with noble metal nanoparticles, RSC Adv. 5 (2015).
[77] X. Zhang, Z. Yao, J. Wang, W. Guo, X. Wu, Z. Jiang, High-capacity NCNT-encapsulated metal NP catalysts on carbonised loofah with dual-reaction centres over C–M bond bridges for Fenton-like degradation of antibiotics, Appl. Catal. B Environ. 307 (2022), 121205.
[78] K. Chhetri, B. Dahal, T. Mukhiya, A.P. Tiwari, A. Muthurasu, T. Kim, H. Kim, H.Y. Kim, Integrated hybrid of graphitic carbon-encapsulated CuxO on multilayered mesoporous carbon from copper MOFs and polyaniline for asymmetric supercapacitor and oxygen reduction reactions, Carbon 179 (2021) 89–99.
[79] P.C. Lohani, A.P. Tiwari, K. Chhetri, A. Muthurasu, B. Dahal, S.-H. Chae, T.H. Ko, J.Y. Lee, Y.S. Chung, H.Y. Kim, Polypyrrole nanotunnels with luminal and abluminal layered double hydroxide nanosheets grown on a carbon cloth for energy storage applications, ACS Appl. Mater. Interfaces 14 (2022) 23285–23296.
[80] M.B. Poudel, A.R. Kim, S. Ramakrishan, N. Logeshwaran, S.K. Ramasamy, H.J. Kim, D.J. Yoo, Integrating the essence of metal organic framework-derived ZnCoTe–N–C/MoS2 cathode and ZnCo-NPS-N-CNT as anode for high-energy density hybrid supercapacitors, Compos. B Eng. 247 (2022), 110339.
[81] H. Dong, C. Liu, H. Ye, L. Hu, B. Fugetsu, W. Dai, Y. Cao, X. Qi, H. Lu, X. Zhang, Three-dimensional nitrogen-doped graphene supported molybdenum disulfide nanoparticles as an advanced catalyst for hydrogen evolution reaction, Sci. Rep. 5 (2015), 17542.

[82] C. Dong, X. Wang, X. Liu, X. Yuan, W. Dong, H. Cui, Y. Duan, F. Huang, In situ grown Nb4N5 nanocrystal on nitrogen-doped graphene as a novel anode for lithium ion battery, RSC Adv. 6 (2016) 81290–81295.
[83] D. He, F. Li, Y. Xiao, S. Chen, Z. Zhu, H. Chen, X. Hu, W. Peng, S. Xin, Y. Bai, Electrostatic self-assembly assisted hydrothermal synthesis of bimetallic NiCo2S4@N, S co-doped graphene for high performance asymmetric supercapacitors, Electrochim. Acta 404 (2022), 139751.
[84] V. Mariyappan, S.-M. Chen, T. Jeyapragasam, J.M. Devi, Designing and construction of a cobalt-metal-organic framework/heteroatoms co-doped reduced graphene oxide mesoporous nanocomposite based efficient electrocatalyst for chlorogenic acid detection, J. Alloys Compd. 898 (2022), 163028.
[85] K.P. Sharma, M. Shin, G.P. Awasthi, C. Yu, Single step hydrothermal synthesis of CuS/MnS composite for electrochemical non-enzymatic glucose sensor, Solid State Sci. 143 (2023), 107279.
[86] S. Chen, W. Liang, X. Wang, Y. Zhao, S. Wang, Z. Li, S. Wang, L. Hou, Y. Jiang, F. Gao, P-doped MOF-derived CoNi bimetallic sulfide electrocatalyst for highly-efficiency overall water splitting, J. Alloys Compd. 931 (2023), 167575.
[87] G.M. Lohar, O.C. Pore, A.V. Fulari, Electrochemical behavior of CuO/rGO nanopellets for flexible supercapacitor, non-enzymatic glucose, and H2O2 sensing application, Ceram. Int. 47 (2021) 16674–16687.
[88] H. Li, Y. Xiong, Y. Wang, W. Ma, J. Fang, X. Li, Q. Han, Y. Liu, C. He, P. Fang, High piezocatalytic capability in CuS/MoS2 nanocomposites using mechanical energy for degrading pollutants, J. Colloid Interface Sci. 609 (2022) 657–666.
[89] X. Wang, L. Li, Z. Fu, F. Cui, Carbon quantum dots decorated CuS nanocomposite for effective degradation of methylene blue and antibacterial performance, J. Mol. Liq. 268 (2018) 578–586.
[90] J. Guo, X. Zhang, Y. Sun, X. Zhang, L. Tang, X. Zhang, Double-shell CuS nanocages as advanced supercapacitor electrode materials, J. Power Sources 355 (2017) 31–35.
[91] P. Fageria, K.Y. Sudharshan, R. Nazir, M. Basu, S. Pande, Decoration of MoS2 on g-C3N4 surface for efficient hydrogen evolution reaction, Electrochim. Acta 258 (2017) 1273–1283.
[92] S. Nisar, M. Tariq, S. Muhammad, M. Saqib, F. Akbar, Electrocatalytic efficacy of Ni-Cu@VC-72: non-enzymatic electrochemical detection of glucose using Ni-Cu nanoparticles loaded on carbon black, Synth. Met. 269 (2020), 116578.
[93] X. Li, H. Dong, Q. Fan, K. Chen, D. Sun, T. Hu, Z. Ni, One-pot, rapid microwave-assisted synthesis of bimetallic metal–organic framework for efficient enzyme-free glucose detection, Microchem. J. 179 (2022), 107468.
[94] S. Arunbalaji, R. Vasudevan, M. Arivanandhan, A. Alsalme, A. Alghamdi, R. Jayavel, CuO/MoS2 nanocomposites for rapid and high sensitive non-enzymatic glucose sensors, Ceram. Int. 46 (2020) 16879–16885.
[95] P. Gao, Y. Zhang, H. Abedi, Hierarchical CuS doped with vanadium nanosheets with micro skein overall morphology as a high performance amperometric glucose sensor, Surface. Interfac. 21 (2020), 100756.
[96] N. Janmee, P. Preechakasedkit, N. Rodthongkum, O. Chailapakul, P. Potiyaraj, N. Ruecha, A non-enzymatic disposable electrochemical sensor based on surface-modified screen-printed electrode CuO-IL/rGO nanocomposite for a single-step determination of glucose in human urine and electrolyte drinks, Anal. Methods 13 (2021) 2796–2803.
[97] M. Yu, X. Ji, F. Ran, Chemically building interpenetrating polymeric networks of Bi-crosslinked hydrogel macromolecules for membrane supercapacitors, Carbohydr. Polym. 255 (2021), 117346.
[98] H. Yang, J. Bao, Y. Qi, J. Zhao, Y. Hu, W. Wu, X. Wu, D. Zhong, D. Huo, C. Hou, A disposable and sensitive non-enzymatic glucose sensor based on 3D graphene/Cu2O modified carbon paper electrode, Anal. Chim. Acta 1135 (2020) 12–19.
[99] J. Shan, J. Li, X. Chu, M. Xu, F. Jin, X. Wang, L. Ma, X. Fang, Z. Wei, X. Wang, High sensitivity glucose detection at extremely low concentrations using a MoS2-based field-effect transistor, RSC Adv. 8 (2018) 7942–7948.
[100] J. Huang, Z. Dong, Y. Li, J. Li, W. Tang, H. Yang, J. Wang, Y. Bao, J. Jin, R. Li, MoS2 nanosheet functionalized with Cu nanoparticles and its application for glucose detection, Mater. Res. Bull. 48 (2013) 4544–4547.
[101] Z. Gao, Y. Lin, Y. He, D. Tang, Enzyme-free amperometric glucose sensor using a glassy carbon electrode modified with poly (vinyl butyral) incorporating a hybrid nanostructure composed of molybdenum disulfide and copper sulfide, Microchim. Acta 184 (2017) 807–814.
[102] X. Zhang, G. Wang, A. Gu, Y. Wei, B. Fang, CuS nanotubes for ultrasensitive nonenzymatic glucose sensors, Chem. Commun. (2008) 5945–5947.
[103] X. Zhang, L. Wang, R. Ji, L. Yu, G. Wang, Nonenzymatic glucose sensor based on Cu–Cu2S nanocomposite electrode, Electrochem. Commun. 24 (2012) 53–56.
[104] N. Batvani, M.A. Tehrani, S. Alimohammadi, M.A. Kiani, Non-enzymatic amperometric glucose sensor based on bimetal-oxide modified carbon fiber ultra-microelectrode, Sensing and Bio-Sensing Research 38 (2022), 100532.